# Post-irradiation annealing behavior of oxide dispersion strengthened Fe-Cr alloys studied by nanoindentation

Duan, B.; Bergner, F.; Heintze, C.; Akhmadaliev, S.; Wang, T.;

Originally published:

April 2019

**Philosophical Magazine Letters 98(2018)12, 536-546**

DOI: https://doi.org/10.1080/09500839.2019.1597990

# Post-irradiation annealing behavior of oxide dispersion strengthened Fe-Cr alloys studied by nanoindentation

Binghuang Duan [a,b], Frank Bergner [b,*], Cornelia Heintze [b], Shavkat Akhmadaliev [b], Tieshan Wang [a]

[a] School of Nuclear Science and Technology, Lanzhou University, Lanzhou 730000, PR China
[b] Helmholtz-Zentrum Dresden-Rossendorf, Bautzner Landstraße 400, 01328 Dresden, Germany

**Abstract**
To study the nature of irradiation-induced nanofeatures in oxide dispersion strengthened (ODS) Fe-Cr alloys, post-irradiation isochronal thermal annealing up to 600 ºC was performed for 9Cr- and 14Cr-ODS alloys ion-irradiated at 300 and 500 ºC. Nanoindentation indicated hardening for all as-irradiated alloys and complete hardness recovery upon post-irradiation annealing. Candidate mechanisms of recovery were critically evaluated. Shrinkage of irradiation-induced dislocation loops via capture of thermal vacancies was found to correctly reflect the behavior of 9Cr-ODS irradiated at 300 ºC.

**Keywords**: ODS steel; Ion irradiation; Post-irradiation annealing; Nanoindentation; Dislocation loops.

## 1. Introduction

Oxide dispersion strengthened (ODS) ferritic-martensitic chromium steels are promising candidates for future nuclear application for their high radiation tolerance [1]. The evolution of irradiation-induced (including ion irradiation) nanofeatures is in the focus of recent interest [2]. Wharry et al. [3] reviewed experimental studies on the evolution of oxide nanoparticles in the Fe-Cr system. While the body of results contains cases of decreasing, stable and increasing size and number density, the nanoparticles tend to be stable for ion irradiations at doses below 10 dpa and temperatures between 300 and 500 °C, e.g. [4]. Tissot et al. [5] recently reported the first observation of α′ phase particles in ion-irradiated samples of an Fe-Cr alloy. These authors also found that the injected interstitials may suppress α′ formation under certain conditions [5]. Dislocation loops have been occasionally investigated in ion-irradiated ODS alloys by using TEM [4,6,7]. De Castro et al. [7] compared the ion-irradiation effects on an ODS 12%Cr steel and a non-ODS reference and found irradiation-induced loops to be smaller for the ODS steel. In [4], loops were observed in an ODS 16%Cr ferritic steel ion-irradiated at 300 °C and suggested to be the dominant source of measured irradiation hardening. Recently, undesired ion-beam-induced carbon contamination and resulting microstructure changes have been reported to occur under a wide range of conditions [8].

Nanoindentation of ion-irradiated Fe-based alloys is a widely accepted technique to study the total effect of microstructure changes on the mechanical properties [4,6,11]. However, it is not

* Corresponding author. E-mail address: f.bergner@hzdr.de

obvious how different types of irradiation-induced nanofeatures, such as those mentioned above, contribute to hardening. To address this issue, the present work aims to gain new insight by studying the effect of post-irradiation isochronal annealing treatments on the nanohardness of ion-irradiated ODS Fe-Cr alloys.

In our previous work [9], irradiation hardening of ODS alloys was investigated on the basis of three-step irradiations with different ion energies for each step to obtain an approximately rectangular damage profile of 10 dpa. The present study is based on nanoindentation in combination with single-step ion irradiation with peak damage of 10 dpa and isochronal post-irradiation thermal annealing. The transition from three-step irradiations, which approximately create rectangular damage profiles, to single-step irradiations, which give rise to graded profiles, was necessary in order to avoid possible annealing effects during the second and third step of the previously applied three-step irradiations. The investigated materials, ion irradiations and isochronal annealing treatments are introduced in the experimental section. Results of nanoindentation measurements are reported. The temperature dependence of hardness recovery and the amount of total recovery are addressed in the discussion section. Candidate mechanisms of recovery are critically evaluated.

## 2. Experiments

The composition of the ODS alloys supplied by CEA, France, is shown in Table 1. 9Cr-ODS-A and -B (code L22-M1) have the same composition and initial fabrication process. The microstructure of 9Cr-ODS-A is ferritic. 9Cr-ODS-B was exposed to an additional heat treatment consisting of austenitization at 1050 ºC for 0.5 h, quenching in oil and tempering at 750 ºC for 1 h. The resulting microstructure is tempered martensite. The microstructure of 14Cr-ODS (code J27-M2) is ferritic. Details on the fabrication processes and initial microstructures have been reported in [9]. One surface of each sample of dimensions 1×10×10 $mm^3$ was mechanically ground with SiC paper (up to 2500 grit), mechanically polished with diamond suspensions down to 1 µm diameter and electro-polished.

**Table 1.** Chemical composition of investigated ODS alloys (data in wt.%, balance Fe).

| Material | Cr | W | Ti | Si | Ni | Mn | added $Y_2O_3$ |
|---|---|---|---|---|---|---|---|
| 9Cr-ODS-A | 9.1 | 1.1 | 0.3 | 0.3 | 0.2 | 0.3 | 0.3 |
| 9Cr-ODS-B | 9.1 | 1.1 | 0.3 | 0.3 | 0.2 | 0.3 | 0.3 |
| 14Cr-ODS | 13.5 | 0.9 | 0.4 | 0.32 | 0.17 | 0.27 | 0.3 |

Ion irradiations were performed with the 3MV-tandetron accelerator at the Ion Beam Center at HZDR. $Fe_2O_3$ was used as Fe-ion source with several independent measures preventing the sample from implantation with oxygen ions. 5MeV-$Fe^{2+}$ ions were implanted into the samples at 300 and 500 ºC. The whole array of samples was scanned by the ion beam. Each sample was masked such that only the central circular area of diameter 8 mm was exposed to ion irradiation. The total fluence was $1.15\times10^{16}$ ions/$cm^2$ with corresponding irradiation time of about 24 h.

Fig. 1 shows the profiles of displacement damage and injected self-interstitials calculated using the SRIM-2008.4 binary collision code according to the recommendations in [10].

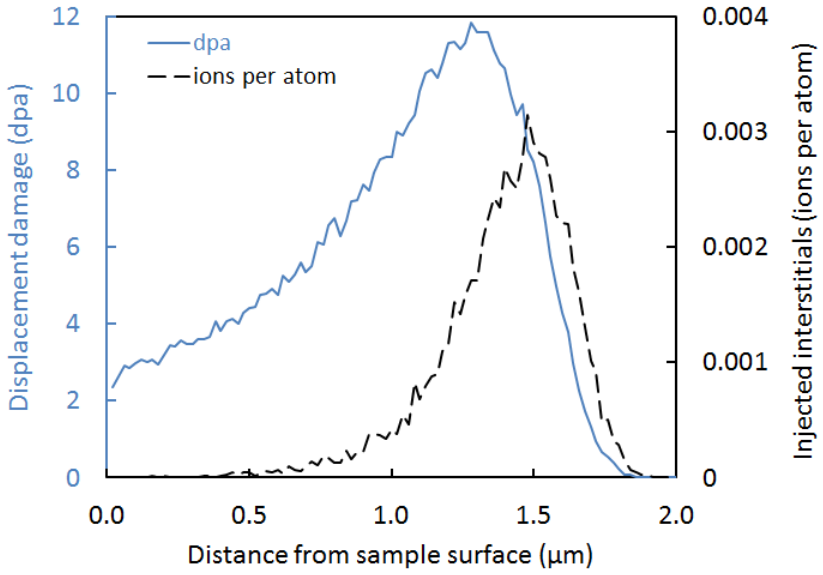


**Fig. 1.** Damage and injected interstitial profiles calculated by SRIM.

The isochronal annealing treatments were performed in a high vacuum furnace under pressure of $5\times10^{-7}$ mbar. The annealing temperatures were chosen from irradiation temperature up to 600 ºC in increments of 50 K with annealing times of 1 h at each temperature.

Nanoindentation hardness $H_{IT}$ was measured using a Universal Nanomechanical Tester (UNAT) equipped with a Berkovich indenter. Quasi continuous stiffness measurement (QCSM) was applied with a maximum load of 100 mN and resulting maximum contact depths $h_C$ of about 1 μm. The $H_{IT}$-$h_c$ plots were calculated by averaging over a minimum of 25 indents. The masked area of each sample was taken as unirradiated reference. It is reasonable to assume that the exposure of the masked areas to the irradiation temperature does not change hardness. The superposition of the initial hardness and the hardness contributed by the irradiation-induced defects was assumed to be linear. The indentation size effect [11] was treated as independent of the effects of irradiation and annealing.

In order to analyze the dependence of the indentation hardness on annealing temperature, the contact depth of 300 nm was chosen as reference depth. As the extension of the plastic zone is approximately seven times larger than the contact depth [12], this choice ensures coverage of the whole depth of the irradiated layer (see Fig. 1) by the plastic zone. The dpa-value averaged over the volume of a hemispherical plastic zone of radius 2.1 μm was calculated to be 5.6 dpa. It is more reasonable to assign this integrated dpa-value instead of the peak value to the hardness data.

## 3. Results

The results of the nanoindentation measurements are summarized in Fig. 2 showing the nanohardness as function of contact depth obtained for the unirradiated, as-irradiated and post-irradiation annealed conditions of the same sample. Comparing the as-irradiated condition and the unirradiated reference, pronounced irradiation hardening is observed for all ODS alloys irradiated at 300 and 500 ºC. To visualize the effects of post-irradiation annealing, the hardness values at the reference depth of 300 nm are plotted as a function of the annealing temperature in Fig. 3. The scatter bands for the unirradiated and as-irradiated conditions are shown for comparison.

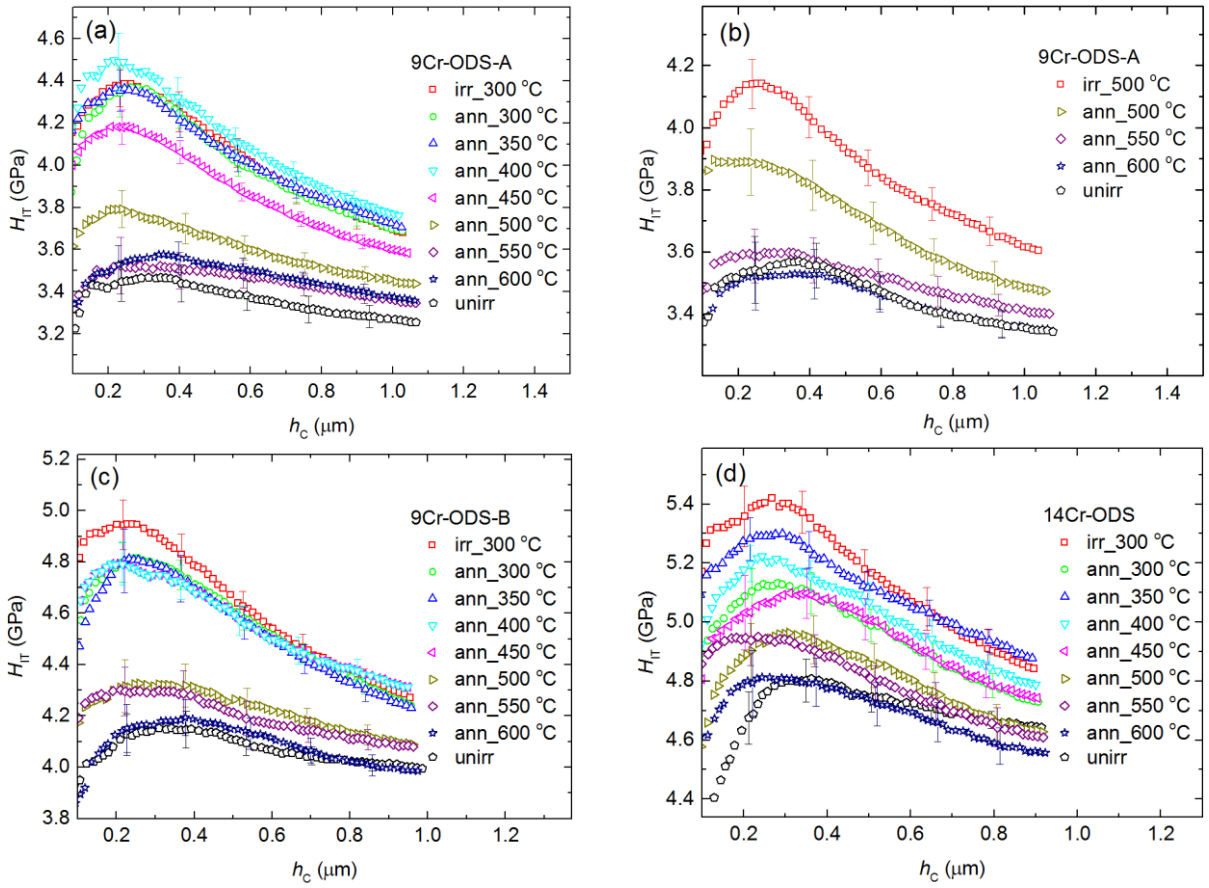


**Fig. 2.** $H_{IT}$-$h_c$ plots measured after irradiation and annealing up to 600 ºC. (a) 9Cr-ODS-A irradiated at 300 ºC; (b) 9Cr-ODS-A irradiated at 500 ºC; (c) 9Cr-ODS-B irradiated at 300 ºC; (d) 14Cr-ODS irradiated at 300 ºC.

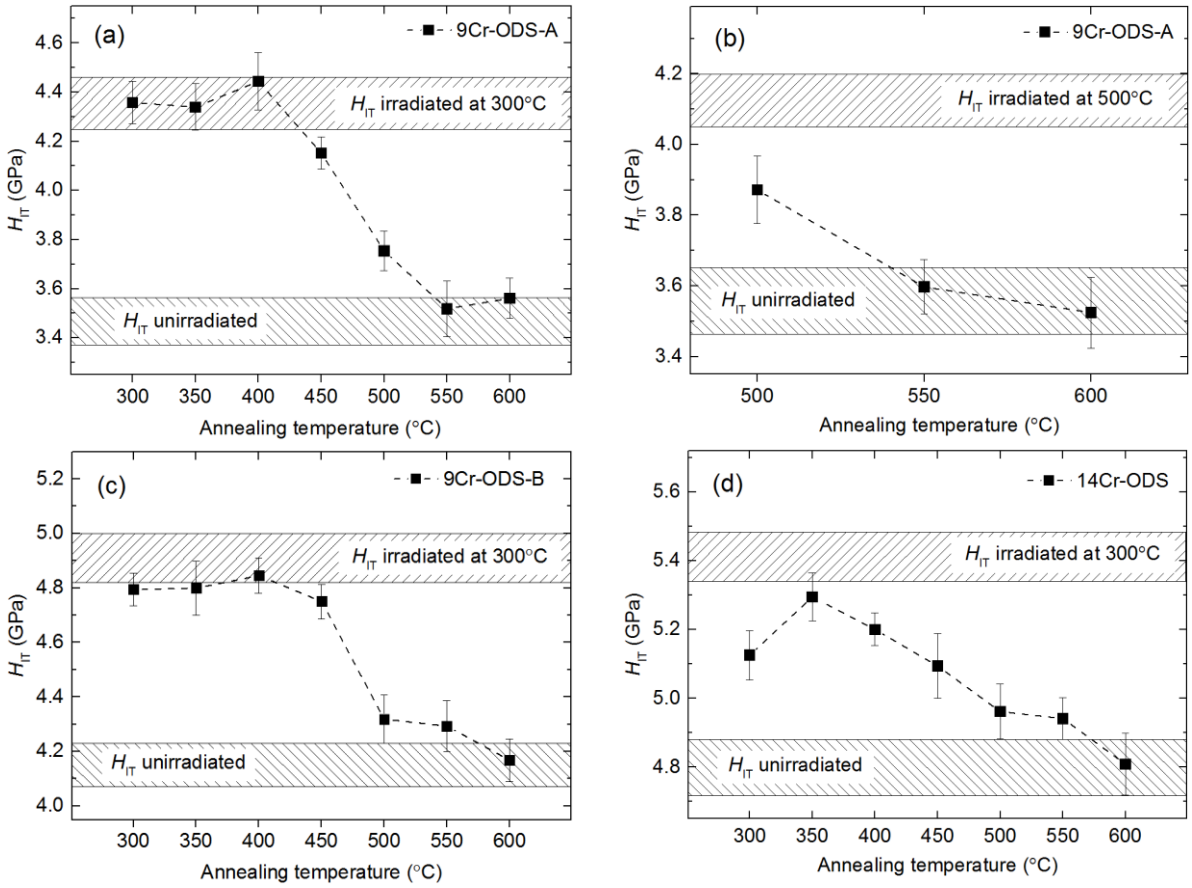


**Fig. 3.** Indentation hardness after isochronal annealing for irradiated 9Cr-ODS-A (a) and (b), 9Cr-ODS-B (c) and 14Cr-ODS (d).

As shown in Figs. 3(a) and (c), the hardness of 9Cr-ODS-A and -B irradiated at 300 ºC remains approximately unchanged (within error) after annealing from 300 to 400 ºC. Substantial hardness decrease occurs in a relatively narrow temperature range between 450 and 550 ºC. Annealing at 600 ºC gives rise to resultant hardness reductions down to the unirradiated reference levels, i.e. complete recovery. As shown in Fig. 3(b), 9Cr-ODS-A irradiated at 500 ºC exhibits a similar annealing behavior except for the remarkable fact that significant hardness reduction was found for the annealing at irradiation temperature. 14Cr-ODS irradiated at 300 ºC exhibits significant hardness reduction after the first annealing step at 300 ºC. Compared with 9Cr-ODS-A and -B, the onset of hardness recovery is observed at lower annealing temperature and the hardness reduction as function of the annealing temperature is smoother. Complete recovery of irradiation-induced hardening is observed after annealing at 600 ºC. It is also important to note that in no case the hardness measured after annealing falls below the respective unirradiated reference.

## 4. Discussion

There are several candidate effects that may be responsible for the irradiation-induced hardening, e.g. formation of dislocation loops, formation of α′-phase particles, changes to the oxide nanoparticles, and effects arising from carbon contamination. The compatibility of these candidate effects with the observed post-irradiation annealing response will be discussed below.

Noticeable changes to the oxide nanoparticles during the present ion irradiations can be largely excluded based on reported evidence [3]. Moreover, irradiation-induced changes to the oxide nanoparticles (if any), e.g. reduction of the mean size, would not be reversed to the initial state as a result of thermal annealing in the applied temperature range because of the high thermal stability of oxide nanoparticles. Therefore, the observed post-irradiation annealing response, in particular complete hardness recovery, confirms that oxide nanoparticles can be ruled out as a substantial contributor to hardening.

Noticeable irradiation-induced formation of α′ phase particles can also be largely excluded for 9Cr-ODS, because, according to the binary Fe-Cr equilibrium phase diagram [13], there is only minor supersaturation at 300 °C and the injected interstitials tend to additionally suppress α′ formation [5]. Irradiation-induced α′ phase particles (again if any) in thermal equilibrium would reduce in volume fraction at increasing temperature and disappear once the annealing temperature exceeds the temperature corresponding to the solubility limit for a given composition. Therefore, irradiation-induced α′ formation followed by thermally induced α′ dissolution is not in a-priori contradiction with the observed complete hardness recovery. However, thermally induced α′ dissolution would run very slowly at annealing temperatures below 500 ºC for kinetic reasons as known from the phenomenon of 475 ºC embrittlement occurring at higher Cr concentrations [14]. Therefore, the observed post-irradiation annealing response also confirms that formation of α′ can be ruled out as a substantial contributor to hardening for the cases of 9Cr-ODS.

For 14Cr-ODS, there is considerable supersaturation at 300 °C and a noticeable amount of α′ may have formed particularly in the sub-μm depth range, which is essentially free of injected interstitials, see Fig. 1. We conclude that thermal dissolution of α′ may play a role in the broadening, as compared to 9Cr-ODS, of the annealing curve for 14Cr-ODS.

The origin and consequences of ion-beam-induced carbon contamination are not yet well understood [8] and may depend on details of the irradiation device. Hardening due to carbon in solution and/or C-Fe(-Cr) complexes or carbides may occur in cases of substantial contamination. However, such contributions would give rise to roughly constant hardness or slight (secondary) hardening upon post-irradiation annealing at temperatures between 200 and 500 °C instead of hardness recovery, as it is well known from the effect of tempering on hardness in quenched and tempered high-Cr steels [15]. Hence, carbon contamination can be ruled out as a source of substantial irradiation-induced hardening in the present case as well.

Vacancy clusters are unlikely to contribute to the observed irradiation hardening because, on the one hand, any vacancy clusters are extremely small [16] and can be ignored [17] for neutron-

irradiated Fe-Cr alloys and, on the other hand, the ion-induced formation of vacancy clusters is additionally penalized by the injected interstitials.

What remains is the effect of dislocation loops. There is convincing evidence for the irradiation-induced formation of dislocation loops in 9-14%Cr ODS and non-ODS Fe-based alloys [4,6,7]. Given the above, it is reasonable to assume that both the irradiation-induced hardening and the annealing response are dominated by the evolution of irradiation-induced loops at least for 9Cr-ODS. To underpin this view, we have applied a model, which is based on the reported evidence that dislocation loops may shrink via capture of thermal vacancies in electron-irradiated pure iron [18] and two steels [19].

According to the model, the shrinkage of loops of radius $r_\mathrm{L}$ is described by Eq. (1) [20],

$$\frac{\mathrm{d}r_\mathrm{L}}{\mathrm{d}t} = -\frac{\Omega}{b} z_\mathrm{vL}(r_\mathrm{L}) D_\mathrm{v} C_\mathrm{v,eq} \tag{1}$$

where $z_\mathrm{vL}(r_\mathrm{L})$ is the capture efficiency of a vacancy by a dislocation loop of radius $r_\mathrm{L}$, $D_\mathrm{v} = D_\mathrm{v0}\exp(-E_\mathrm{m}/k_\mathrm{B}T)$ is the diffusion coefficient of vacancies in iron, $C_\mathrm{v,eq} = \exp(-E_\mathrm{f}/k_\mathrm{B}T)$ is the concentration of vacancies in iron at thermal equilibrium and *T* is the absolute temperature. For the meaning of the symbols, see also Table 2. It is important to note that, in spite of the capture of vacancies, the thermal equilibrium concentration is maintained by way of spontaneous emission of vacancies from point defect sources such as grain boundaries. An expression discussed in [21] is applied for $z_\mathrm{vL}$, Eq. (2), in which the toroidal shape of loops is taken into account.

$$z_\mathrm{vL}(r_\mathrm{L}) = \frac{2\pi}{ln(4r_\mathrm{L}/b)} \tag{2}$$

This approximation is applicable for not too large loops [21] as justified in the present case. The resulting equation can be solved by separation of variables to give an implicit equation describing the shrinkage of loops of initial radius $r_\mathrm{L0}$ as function of annealing time *t*. A loop size less than about 0.2 nm is physically meaningless and interpreted in terms of reduction of loop number density $N_\mathrm{L}$. Application of the dispersed barrier hardening model [17], Eq. (3), along with the conversion of yield stress to indentation hardness allows the hardness recovery during annealing to be roughly estimated. The reported values of the physical parameters introduced above are summarized in Table 2.

$$\Delta H_\mathrm{IT} = \alpha\beta MGb\sqrt{2N_\mathrm{L}r_\mathrm{L}} \tag{3}$$

**Table 2**. Set of parameters used in Eqs. (1)-(3).

| Parameter | Value | Source |
|---|---|---|
| Atomic volume of Fe, $\Omega$ | $1.2\times10^{-29}$ m$^3$ | [22] |
| Pre-factor, $D_\mathrm{v0}$ | $10^{-4}$ m$^2$/s | [21] |
| Vacancy migration energy, $E_\mathrm{m}$ | 1.25 eV * | [23] |

| | | |
|---|---|---|
| Vacancy formation energy, $E_f$ | 1.6 eV | [21] |
| Obstacle strength of loops, $\alpha$ | 0.3 | [17] |
| Conversion factor, $\beta$ | 3.8 | ** |
| Taylor factor, $M$ | 3.06 | [17, 24] |
| Burgers vector, $b$ | 0.248 nm | [17] |
| Shear modulus of Fe, $G$ | 84 GPa | [17] |

* Optimum value taking into account the effect of carbon-vacancy complexes [23].
** This work (based on unirradiated conditions only).

The calculations show that the dependence of the loop size on annealing temperature only weakly depends on the initial loop size in the relevant size range. This allows the initial size distribution of loops to be represented by the mean radius, which is taken to be 2 nm as reported in [7] for an ODS Fe-12Cr alloy irradiated with Fe ions. The total initial number density of loops $N_{L0}$ was calculated in such a way that the irradiation-induced hardness increase $\Delta H_{IT}$ according to Eq. (3) coincides with the hardness increase measured for 9Cr-ODS-A. The calculated value, $N_{L0}$ = 4 x $10^{-5}$ $nm^{-3}$, is of reasonable order of magnitude. The shrinkage of loops after 1 h of annealing was derived from Eq. (1) and used to calculate the hardness according to Eq. (3). A comparison of the calculated (red triangles) and measured results for 9Cr-ODS-A irradiated at 300 ºC is shown in Fig. 4.

The observed hardness recovery in a narrow temperature range is reflected well by the model. We have found that the temperature range of steep hardness decrease is dominated by the parameters $E_m$ and $E_f$. From a discussion of the reported values of $E_m$ and $E_f$ [21], the former can be identified as possible source of discrepancy between measurement and calculation. Indeed, a slight reduction of $E_m$, still in the reported range [21], yields a better fit (green squares). The same parametrization of the model is also applicable to 9Cr-ODS-B if the measured irradiation-induced hardness increase is applied. Obviously, the pre-irradiation microstructure (ferritic versus martensitic) does not essentially alter the mechanism of hardness recovery.

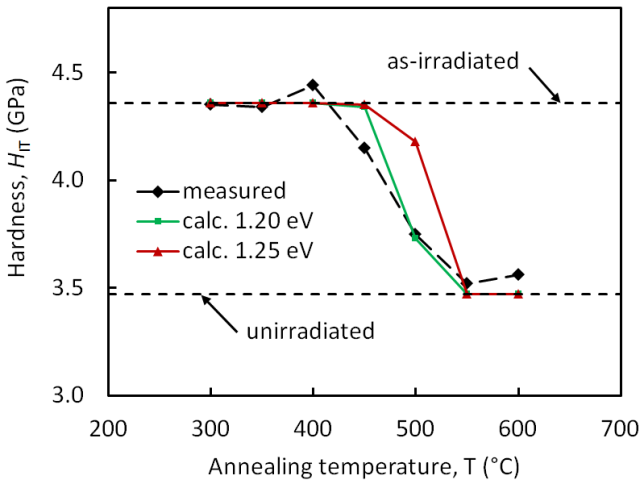


**Fig. 4.** Comparison of the measured and calculated hardness for 9Cr-ODS-A annealed for 1 h as function of annealing temperature. The values of $E_m$ used for the calculations are indicated.

14Cr-ODS irradiated at 300 ºC exhibits a distinctly different response to post-irradiation annealing, as shown in Fig. 3(d). The range of annealing temperatures in which hardness recovery takes place is broader than that of 9Cr-ODS-A and -B. While it is reasonable to assume that shrinkage of loops plays a role in the hardness recovery in 14Cr-ODS as well, two competing mechanisms seem to operate. Irradiation-induced α′ formation followed by thermally induced α′ dissolution has been identified above as second candidate.

## 5. Conclusion

The effect of post-irradiation isochronal annealing on nanohardness was studied for 9Cr- and 14Cr-ODS alloys self-ion irradiated at 300 ºC and (for 9Cr) 500 ºC in order to gain additional insight on the dominant sources of hardening. While the annealing response allows a number of possible hardening mechanisms to be ruled out, the shrinkage and disappearance of irradiation-induced loops via capture of thermal vacancies is consistent with the hardness recovery observed for 9Cr-ODS. For 14Cr-ODS, two mechanisms of irradiation hardening seem to compete.

**Acknowledgement**
This work was supported by the EU-FP7 project MatISSE (Grant Agreement No. 604862). The first author appreciates funding from the China Scholarship Council. Access to the Ion Beam Center of HZDR is gratefully acknowledged.

## References

[1] S. Ukai and M. Fujiwara, J. Nucl. Mater. 307–311 (2002) pp.749-757.
[2] T. Chen, H. Kim, J.G. Gigax, D. Chen, C.-C. Wei, F.A. Garner and L. Shao, Nucl. Instrum. Methods Phys. Res. B (2017) pp.259-263.
[3] J.P. Wharry, M.J. Swenson and K.H. Yano, J. Nucl. Mater. 486 (2017) pp.11-20.
[4] K. Yutani, R. Kasada, H. Kishimoto and A. Kimura, J. ASTM Int. 4 (2007) pp.323-328.
[5] O. Tissot, C. Pareige, E. Meslin, B. Décamps and J. Henry, Mater. Res. Lett. (2016) pp.1-7.
[6] C. Liu, C. Yu, N. Hashimoto, S. Ohnuki, M. Ando, K. Shiba and S. Jitsukawa, J. Nucl. Mater. 417 (2011) pp.270-273.
[7] V. de Castro, S. Lozano-Perez, M. Briceno, P. Trocellier, S.G. Roberts and R. Pareja, J. Mater. Sci. 50 (2015) pp.2306-2317.
[8] G.S. Was, S. Taller, Z. Jiao, A.M. Monterrosa, D. Woodley, D. Jennings, T. Kubley, F. Naab, O. Toader and E. Uberseder, Nucl. Instrum. Methods Phys. Res. B 412 (2017) pp.58-65.
[9] B. Duan, C. Heintze, F. Bergner, A. Ulbricht, S. Akhmadaliev, E. Oñorbe, Y. de Carlan and T. Wang, J. Nucl. Mater. 495 (2017) pp.118-127.
[10] R.E. Stoller, M.B. Toloczko, G.S. Was, A.G. Certain, S. Dwaraknath and F.A. Garner, Nucl. Instrum. Methods Phys. Res. B 310 (2013) pp.75-80.
[11] W.D. Nix and H. Gao, J. Mech. Phys. Solids 46 (1998) pp.411-425.
[12] C. Heintze, C. Recknagel, F. Bergner, M. Hernández-Mayoral and A. Kolitsch, Nucl. Instrum. Methods Phys. Res. B 267 (2009) pp.1505-1508.

[13] G. Bonny, D. Terentyev and L. Malerba, J. Phase Equilib. Diff. 31 (2010) pp.439-444.
[14] P.J. Grobner, Metall. Trans. 4 (1973) pp.251-260.
[15] H. Bhadeshia and R. Honeycombe, *Steels: Microstructure and Properties (Fourth edition)*, Butterworth-Heinemann, 2017, p.259.
[16] M. Lambrecht and L. Malerba, Acta Mater. 59 (2011) pp.6547-6555.
[17] F. Bergner, C. Pareige, M. Hernández-Mayoral, L. Malerba and C. Heintze, J. Nucl. Mater. 448 (2014) pp.96-102.
[18] M. Kiritani, H. Takata, K. Moriyama and F.E. Fujita, Philos. Mag. A 40 (1979) pp.779-802.
[19] N. Hashimoto, S. Goto, S. Inoue and E. Suzuki, J. Nucl. Mater. 495 (2017) pp.1-5.
[20] G.S. Was, *Fundamentals of radiation materials science : metals and alloys*, Springer, Berlin ; New York, 2007.
[21] A.H. Duparc, C. Moingeon, N. Smetniansky-de-Grande and A. Barbu, J. Nucl. Mater. 302 (2002) pp.143-155.
[22] Z.N. Ding, C.H. Zhang, Y.T. Yang, Y. Song, A. Kimura and J. Jang, J. Nucl. Mater. 493 (2017) pp.53-61.
[23] C.C. Fu, E. Meslin, A. Barbu, F. Willaime and V. Oison, Solid State Phenomena 39 (2008), pp.157-164.
[24] J.T. Busby, M.M. Sowa, G.S. Was and E.P. Simonen, Philos. Mag. 85 (2005) pp.609-617.